HHS Public Access

Author manuscript

Biomaterials. Author manuscript; available in PMC 2020 May 01.

Published in final edited form as:

Biomaterials. 2019 May ; 201: 1–15. doi:10.1016/j.biomaterials.2019.01.039.

Surface Tethering of Stem Cells with H_2O_2-Responsive Anti-Oxidizing Colloidal Particles for Protection Against Oxidation-Induced Death

Jye Yng Teo[a,b], **Yongbeom Seo**[a], **Eunkyung Ko**[c], **Jiayu Leong**[a,b], **Yu-Tong Hong**[a], **Yi Yan Yang**[b], and **Hyunjoon Kong**[a,c,d,e,*]

[a]Department of Chemical and Biomolecular Engineering, University of Illinois at Urbana-Champaign, Urbana, IL 61801, USA

[b]Institute of Bioengineering and Nanotechnology, 31 Biopolis Way, The Nanos, Singapore 138669, Singapore

[c]Department of Bioengineering, University of Illinois at Urbana-Champaign, Urbana, IL 61801, USA

[d]Carl R. Woese Institute for Genomic Biology, University of Illinois at Urbana-Champaign, Urbana, IL 61801, USA

[e]Carle Illinois College of Medicine, University of Illinois at Urbana-Champaign, Urbana, IL, 61801, USA

Abstract

Mesenchymal stem cells are the new generation of medicine for treating numerous vascular diseases and tissue defects because of their ability to secrete therapeutic factors. Poor cellular survival in an oxidative diseased tissue, however, hinders the therapeutic efficacy. To this end, we hypothesized that tethering the surface of stem cells with colloidal particles capable of discharging antioxidant cargos in response to elevated levels of hydrogen peroxide (H_2O_2) would maintain survival and therapeutic activity of the stem cells. We examined this hypothesis by encapsulating epigallocatechin gallate (EGCG) and manganese oxide (MnO_2) nanocatalysts into particles comprising poly(D,L-lactide-*co*-glycolide)-block-hyaluronic acid. The MnO_2 nanocatalysts catalyzed the decomposition of H_2O_2 into oxygen gas, which increased the internal pressure of particles and accelerated the release of EGCG by 1.5-fold. Consequently, stem cells exhibited 1.2-fold higher metabolic activity and 2.8-fold higher secretion level of pro-angiogenic factor in sub-lethal H_2O_2 concentrations. These stem cells, in turn, performed a greater angiogenic potential

*Corresponding author: Hyunjoon Kong; Phone number: (217) 333-1178; hjkong06@illinois.edu.

Data Availability

All the data required to reproduce this work and validate the conclusion are presented in the paper and Supplementary Materials. The raw/processed data required to reproduce these findings cannot be shared at this time as the data also forms part of an ongoing study.

with doubled number of newly formed mature blood vessels. We envisage that the results of this study will contribute to improving the therapeutic efficacy of a wide array of stem cells.

Keywords

Mesenchymal stem cells; Epigallocatechin gallate; Manganese oxide nanocatalysts; Colloidal particles; Surface tethering; Hydrogen peroxide

1. Introduction

Mesenchymal stem cells are non-hematopoietic fibroblast-like cells which can be isolated from the bone marrow, peripheral blood and adipose tissues [1,2]. As the major stem cells for cell-based therapy, mesenchymal stem cells hold great promises in treating numerous vascular pathological conditions such as ischemia and tissue injury. These cells are known to secrete a diverse repertoire of growth factors such as vascular endothelial growth factor (VEGF), fibroblast-like growth factors, insulin-like growth factors, and pigment epithelium-derived factor which serve to promote balanced tissue regeneration [3–5]. In addition, mesenchymal stem cells release immunomodulatory cytokines such as interleukin 10, interleukin 6, and transforming growth factor beta to suppress the activation and proliferation of immune cells [2–5].

Despite the potential advantages of mesenchymal stem cells, low therapeutic efficacy due to poor survival of the transplanted cells in the injured tissues remains as the largest obstacle in the stem cell therapy [6]. Cell tracking studies using positron emission tomography showed low retention of the transplanted mesenchymal stem cells (i.e.~6%) in the porcine ischemic heart muscle after 10 days of post injection [7]. Similarly, in murine models of hindlimb ischemia using bioluminescence imaging, only a small portion of mesenchymal stem cells survived after transplantation [8].

This impaired therapeutic activity of mesenchymal stem cells at the injured tissues is often related to the abnormally high oxidative stress that triggers cell apoptosis. In response to hypoxia arising from ischemia injury, the electron transport chain in mitochondria of residential cells undergoes conformational changes which facilitate the leakage of electrons [9–11]. This in turn increases the reduction of molecular oxygen to superoxide anion and dismutation to hydrogen peroxide (H_2O_2) [11,12]. H_2O_2 permeates into cells and can react with ferrous iron in cytoplasm to produce hydroxyl radical, the most reactive form of radical [12–14]. These reactive oxygen species (ROS) are unstable, thus react with the biological molecules inside the cells [14,15].

As an innate defense mechanism against ROS-induced damage, cells utilize antioxidant enzymes such as glutathione peroxidases and catalases for the conversion of H_2O_2 into water and oxygen [14,16]. Overproduction of ROS in the injured tissues can overwhelm the intrinsic antioxidant capability of cells and lead to apoptosis when the free radicals irreversibly inactivate the intracellular biological molecules [16]. In the case of mesenchymal stem cells, studies have revealed that H_2O_2 induces apoptosis *via* the endoplasmic reticulum and mitochondrial pathways activated by protein kinases Jun N-

terminal kinase and p38 [17]. Consequently, the transplanted stem cells would not be able to secrete the desired therapeutic cytokines and growth factors.

To improve the survival of these stem cells at the injured tissues, efforts have been made to precondition the cells with antioxidants agents *in vitro* before transplantation. Preconditioning of cells entails cellular incubation in culture media supplemented with the antioxidants of interest for a period of time [18]. Epigallocatechin gallate (EGCG), which is naturally derived from green tea leaves, is one promising antioxidant [19,20]. When exposed to H_2O_2 solution, mesenchymal stem cells pre-treated with EGCG exhibited significantly lower intracellular oxidative stress and higher viability than those without EGCG pretreatment [19]. EGCG helps cells mitigate oxidative stress by oxidizing the D ring of its galloyl group and increasing the activity of the antioxidant enzymes in the cells [19,20]. The cell culture media, however, often contains animal-derived products (e.g. fetal or horse serum) and may elicit unwanted xenogeneic immune responses in the long run [21].

To this end, we hypothesized that colloidal particles devised to anchor to stem cell surface and discharge antioxidant cargos in the presence of H_2O_2 would prolong cellular survival and maintain the therapeutic activity of mesenchymal stem cells in the transplanted site (Figure 1). We examined this hypothesis by encapsulating EGCG molecules into particles assembled with the block copolymer of poly(D,L-lactide-*co*-glycolide) and CD44-binding hyaluronic acid (denoted as PLGA-*b*-HA). PLGA-*b*-HA particles were loaded with MnO_2 nanocatalysts to render them responsive to H_2O_2. At elevated levels of H_2O_2, MnO_2 nanocatalysts served to increase the internal pressure of particles by decomposing the H_2O_2 to O_2 [22]. The pressure increment acts as a pump that would release the EGCG molecules continuously.

Specifically, we tethered these H_2O_2-reponsive anti-oxidizing particles to human adipose tissue-derived mesenchymal stem cells. Then, we evaluated the release rate of EGCG from the particles while incubating them in the physiological media supplemented with H_2O_2. We also assessed the spatial distribution and binding affinity of these particles to the surface of stem cells. We next examined the extent to which these particles modulated the metabolic activity, the secretion activity, the intracellular oxidative stress level, and the glutathione peroxidase activity of the stem cells in an oxidative environment. Finally, mesenchymal stem cells exposed to H_2O_2 were transplanted onto the chick chorioallantoic membrane to evaluate the angiogenic potential of the stem cells.

2. Materials and Methods

2.1. Materials

All chemicals were obtained from Sigma-Aldrich (U.S.A.), and used as received unless specified. Hyaluronic acid (HA) of molecular weights 10kDa was purchased from Lifecore Biomedical (U.S.A.). PLGA with an acid end group and molecular weights ranging from 6,000 to 10,000 g/mol (ratio of lactic: glycolic =50:50) was bought from LACTEL Absorbable Polymers, DURECT (U.S.A). Bovine collagen solution (PureCol®, Type 1) was purchased from Advanced Biomatrix. The reconstituting solution for gelation of collagen was formulated as a mixture of sodium bicarbonate (0.26 M), 4-(2-hydroxyethyl)-1-

piperazineethanesulfonic acid (HEPES, 0.2 M) and sodium hydroxide (0.04 N). Sodium 2,3,-bis(2-methoxy-4-nitro-5-sulfophenyl)-5-[(phenylamino)-carbonyl]-2H-tetrazolium inner salt (XTT) cell proliferation kit and CellROX® Green Reagent were obtained from Trevigen (U.S.A.) and ThermoFisher Scientific (U.S.A.), respectively. DAPI was purchased from Invitrogen™ (U.S.A.). Rhodamine B conjugated bovine serum albumin (BSA-Rhodamine B) was prepared by reacting 1 mg/mL of Rhodamine B isothiocyanate (dissolved in DMSO) with 6 mg/mL of BSA (dissolved in 0.1 M sodium bicarbonate buffer, pH 9.2). BSA-Rhodamine B was purified *via* dialysis against water and lyophilized prior to usage. All experiments involving BSA-Rhodamine B were performed in the dark.

2.2. Cell Culture

Human adipose-derived mesenchymal stem cells were purchased from Lonza (U.S.A.) and cultured in Minimum Essential Medium Alpha Medium (Corning, U.S.A.) containing 2 mM L-Glutamine and sodium pyruvate (Lonza, U.S.A) supplemented with 10% fetal bovine serum (FBS, Life Technologies, U.S.A.), 100 U/mL penicillin (Lonza, U.S.A.) and 100 μg/ml streptomycin (Lonza, U.S.A.) at 37 °C in 5% CO_2 atmosphere. All cellular experiments were conducted using adipose-derived mesenchymal stem cells of passage 6 or lower. Culture media without sodium pyruvate was used whenever hydrogen peroxide was involved.

2.3. Synthesis of PLGA-*b*-HA and Fabrication of H_2O_2-Responsive Anti-Oxidizing Particles

Block copolymers of PLGA and HA were synthesized using an end-to-end coupling strategy [23]. Briefly, N-hydroxysuccinimide-functionalized PLGA (120 mg, 1.5×10^{-5} mol) was reacted with amino-functionalized HA (150 mg, 1×10^{-5} mol) in dimethyl sulfoxide for 48 h at 50 °C under stirring. N, N-diisopropylethylamine (4.4 μL, 2.5×10^{-5} mol) was charged to the reaction vial. The resulting PLGA-*b*-HA was purified *via* dialysis against 4 L of DI water using a dialysis bag with a molecular weight cut-off of 10,000 Da (Spectra/Por 7, Spectrum Laboratories Inc.). Water was changed twice a day for 2 days before lyophilizing.

The H_2O_2-responsive anti-oxidizing particles were fabricated *via* the double emulsification. Briefly, 10 mg of PLGA-*b*-HA was dissolved in an organic mixture of dimethylformamide (DMF) and dichloromethane (DCM) at a volume ratio of 1:3 under bath sonication at room temperature for ~1 h. DMF, which is more polar than DCM, helps with the dissolution of the HA blocks in PLGA-*b*-HA.

MnO_2 nanocatalysts were prepared by dissolving $KMnO_4$ (50 mM, 500 μL) into alginate solution (2.0 % w/v in 0.2 M MES buffer at pH 6.0, 500 μL). EGCG (1 mg/mL in 25 mM MnO_2 nanocatalysts, 200 μL) was added to the organic phase of polymer, and immediately sonicated in an ice-bath for 30 sec using a probe-based sonicator (Fisher Scientific Sonic Dismembrator Model 100, U.S.A.) followed by vortexing for 30 sec (Scientific Industries, Inc, U.S.A.). This process of probe-based sonication and vortexing was repeated twice to yield the first emulsion. The second emulsion was produced by adding the first W/O emulsion into an aqueous solution of polyvinyl alcohol (1% v/v PVA). The mixture was sonicated in ice-bath followed by vortexing for three rounds. The DMF-DCM solvent was

subsequently removed by stirring for 4 h at room temperature. The particles were then washed once in DI water *via* centrifugation and used for further studies or lyophilized for 2 days.

2.4. Physical Characterization of the H_2O_2-Responsive Anti-oxidizing Particles

2.4.1. Morphological Analysis—The morphologies of freshly prepared H_2O_2-responsive anti-oxidizing particles were analyzed by transmission electron microscopy (JEOL 2100 Cryo TEM, U.S.A.) using an acceleration voltage of 200 keV. A drop of the particle solution (10.0 μL) was added onto a carbon film 200 mesh copper grid (Electron Microscopy Sciences, U.S.A.) and left to dry at room temperature overnight.

2.4.2. Analysis of Encapsulation Efficiency of EGCG and MnO_2 nanocatalysts, *in vitro* release of EGCG and Reactivity to H_2O_2—Encapsulation efficiency of EGCG in the particles was quantified by centrifugation of the particles (10 mg/mL) at 12,000 rpm for 5 min at the designated time points. The absorbance of EGCG in the supernatant was measured at 230 nm using a microplate reader (TECAN Infinite® M200 Pro, Switzerland). Three replicates were evaluated. A linear curve of absorbance against concentration of EGCG was plotted. The actual mass of EGCG encapsulated in the particles was calculated from the difference between the initial feeding mass of 0.2 mg and the mass of EGCG present in the supernatant. The amount of MnO_2 nanocatalysts within the particles was calculated by quantifying the number of manganese atoms with inductively coupled plasma atomic emission spectroscopy analysis. The respective encapsulation efficiency of EGCG and MnO_2 nanocatalysts was subsequently determined with the following equation:

$$Encapsulation\ efficiency = \frac{Actual\ mass\ of\ cargos\ in\ particles}{Feeding\ mass\ of\ cargos} \times 100\%$$

The release profile of EGCG was obtained by incubating the H_2O_2-responsive anti-oxidizing particles and particles loading EGCG only in PBS mixed with 0 or 200 μM H_2O_2. The particle concentration was kept constant at 10 mg/mL. The particle suspension was shaking at 100 rpm and the temperature was held constant at 37 °C. At the designated time points, the particles were centrifuged at 12,000 rpm for 5 min at room temperature. The entire supernatant was collected to measure the absorbance of EGCG released from the particles at 230 nm. Separately, the concentration of H_2O_2 in the supernatant was quantified by using Pierce™ Quantitative Peroxide Assay Kit (Thermo Scientific, U.S.A.) which measures the amount of purple product formed from the complexation of Fe^{3+} and xylenol orange at an absorbance of 560 nm. The concentration of Fe^{3+}, which is produced from the redox reaction between Fe^{2+} and H_2O_2, is proportional to the concentration of H_2O_2. The particles were then resuspended with 1 mL of fresh PBS with or without the H_2O_2.

2.5. Analysis of Spatial Distribution of PLGA-*b*-HA Particles on MSCs and Cellular Uptake

PLGA-*b*-HA particles were fluorescently labeled by loading BSA-Rhodamine B. These fluorescently labeled particles (33 mg/mL, 100 μL) were mixed with MSCs (1×10^5 cells/mL) in suspension for 15 min at room temperature. The mixture was subsequently centrifuged to remove unbound particles in the supernatant. The cell pellet was then

resuspended with PBS and seeded immediately on glass slides sandwiched with coverslips for confocal imaging (Carl Zeiss LSM 700, Germany). To examine the possibility of cellular uptake, the cell pellet was resuspended in cell media and seeded on coverslips over a period of 72 h. The nuclei and plasma membrane of the cells were stained with Hoechst 33342 (5 μg/mL, Thermo Fisher Scientific, U.S.A.) and DiO (25 ng/ml, Invitrogen, U.S.A.). The excitation wavelength (λ_{ex}) and emission wavelength (λ_{em}) of each probe were as follows: Hoechst 33342 (λ_{ex}: 350 nm, λ_{em}: 470 nm), DiO (λ_{ex}: 480 nm, λ_{em}: 520 nm), Rhodamine B (λ_{ex}: 532 nm, λ_{em}: 625 nm).

2.6. Analysis of Detachment of Particles from MSCs following Injection

PLGA-*b*-HA particles were fluorescently labeled by loading BSA-Rhodamine B. These fluorescently labeled particles (2.5 mg) were mixed with MSCs (2×10^5 cells) in suspension for 15 min at room temperature. The mixture was subsequently centrifuged to remove unbound particles in the supernatant. The cell pellet was then resuspended with PBS and the cell suspension was injected through a syringe with a needle (26G, ½ inch) using a syringe pump (KDS 100 Legacy Single Syringe Infusion Pump, U.S.A.). The flow rate was controlled at 1.5 mL/min. The cell suspension was then collected at the end of the needle and centrifuged. The fluorescence intensity of the detached particles in the supernatant was measured at a wavelength of 590 nm using microplate reader (TECAN Infinite® M200, Switzerland). Three replicates were tested.

2.7. Seeding of MSCs in Collagen Gel and Exposure to H_2O_2

MSCs were tethered with the particles and seeded in a bovine Type I collagen gel. The volume ratio among gel, cell suspension in pyruvate free media and reconstituting solution was kept constant at 8:4:1 [24]. The reconstituting solution comprises sodium hydrogen carbonate (0.26 M), 4-(2-hydroxyethyl)-1-piperazineethanesulfonic acid (0.2 M), and sodium hydroxide (0.04 N). The cell-loaded collagen was prepared in 96-well plates. The cell density was kept constant at 15,000 cells per gel with a volume of 100 μL. Following the gelation of collagen at 37 °C under an atmosphere of 5% CO_2, the cells were either incubated with H_2O_2-supplemented cell culture media (200 μM H_2O_2, 100 μL/well) or H_2O_2-free media for 2 h. The solution was subsequently removed and replaced with fresh medium.

2.8. Analysis of Metabolic Activity of MSCs

The ability of the H_2O_2-responsive anti-oxidizing particles to maintain the metabolic activity of MSCs in H_2O_2-supplemented media was assessed through the XTT assay. Following the removal of H_2O_2, XTT assay was either performed immediately or on Days 1 and 4. 50 μL of XTT solution comprising XTT activator and XTT reagent (1: 50 v/v) was added to 100 μL of culture medium in each well. The plates were maintained at 37 °C under an atmosphere of 5% CO_2 for 3 h before measuring the absorbance at 490 nm with a reference wavelength of 630 nm. Three replicates were tested for each condition.

2.9. Analysis of Cell Shape Index of MSCs

The morphology of the MSCs seeded in the collagen gel on Day 4 was captured using an inverted microscope (Leica DMi1, Germany) installed with imaging software Leica Application Suite. The cell shape index (CSI) of the cells was then calculated by using ImageJ Software from the projected 2D images of the cells. Briefly, the periphery of individual cells was outlined manually to compute the area (A) and perimeter (P). CSI was then quantified as $CSI = \frac{4\pi A}{P^2}$. A minimum of 50 cells was quantified per condition.

2.9. Analysis of Secretion Activity of MSCs

The ability of MSCs to secrete vascular endothelial growth factor (VEGF) was determined using a Human DuoSet VEGF enzyme-linked immunosorbent assay (ELISA) kit (R&D Systems, U.S.A.). The cell culture media from each well of a 96-well plate was collected on Days 1 and 4. The volume of the cell culture supernates was monitored visually on a daily basis to ensure no/minimal loss. The collected supernates were then incubated with the given Capture Antibody (diluted in PBS) overnight at room temperature. After removal of the Capture Antibody and washing of the plates with PBS containing 0.05% Tween 20, Regent Diluent was added to the plates to block free binding sites. Diluted supernates and standards (100 μL/well) were added to the plates and incubated for 2 h at room temperature. Following thorough washing, biotinylated Detection Antibody (diluted in Regent Diluent) was introduced for 2 h before adding Streptavidin conjugated to Horse Radish Peroxidase to each well. Substrate Solution comprising H_2O_2 and tetramethylbenzidine was added subsequently to the plates for 20 min at room temperature and was followed by the addition of Stop Solution (2N H_2SO_4) to quench the reaction. The optical density of each well was measured immediately at an absorbance wavelength of 450 nm using the microplate reader (TECAN® Infinite M200 Pro, Switzerland). A correction wavelength of 570 nm was used to account for optical imperfections.

2.10. Analysis of Intracellular Oxidative Stress Level of MSCs

The level of oxidative stress in MSCs was assessed using CellROX® Green Reagent. Prior to the end of the 2 hour-H_2O_2 exposure, CellROX® Green Reagent (10 μM) was added to the culture media in each well containing cells seeded in the collagen gel and incubated for 30 min at 37 °C under an atmosphere of 5% CO_2. The cells were subsequently fixed with 3.7% formaldehyde for 20 min at room temperature before DAPI staining (300 μM) for 20 min at room temperature. The samples were washed with PBS and transferred onto clean glass slides gently sandwiched with coverslips for the confocal laser scanning microscopy (Carl Zeiss LSM 700, Germany). The excitation/emission wavelengths of DAPI and CellROX® Green Reagent were 405 nm/435 nm and 488 nm/520 nm, respectively. All observations were conducted under the same instrumental settings. ImageJ software was then utilized to quantify the mean gray value of CellROX® Green Reagent per stem cell. A minimum of 5 individual cells was evaluated per condition.

2.11. Analysis of Glutathione Peroxidase Activity in MSCs

The activity of glutathione peroxidase (GPx) in the stem cells was examined using a Glutathione Peroxidase Activity Colorimetric Assay kit (BioVision. Inc., U.S.A.). MSCs of various conditions were seeded in collagen gel in 24-well plates at a density of 50,000 cells per gel volume of 300 μL. Following 2 h incubation in H_2O_2-supplemented media at 200 μM H_2O_2, the cells were washed once with cold PBS and homogenized with hypodermic needles (28G) in cold Assay Buffer (BioVision, K762-100-1) on ice. The cell homogenates were collected and centrifuged at 10,000 g for 15 min at 4°C. The supernatant samples were then collected in cold tubes and stored on ice. 50 μL of the samples (diluted in cold Assay Buffer) or Assay Buffer (as control) was added into each well of 96-well plates before preparation of the Reaction Mix comprising the Assay Buffer, Nicotinamide Adenine Dinucleotide Phosphate (NADPH) solution, glutathione reductase, and reduced glutathione. 40 μL of the Reaction Mix was subsequently added to each well followed by the addition of 10 μL of cumene hydroperoxide to start the depletion reaction of GPx (proportional to the concentration of NADPH). The optical density (OD_{340}) of NADPH was measured at 340 nm using a microplate reader (TECAN® Infinite M200 Pro, Switzerland). NADPH standard curve was generated by plotting the OD_{340} values against the respective concentration of NADPH (in nmol). An OD_{340} higher than 1.0 was obtained by addition of NADPH before adding cumene hydroperoxide. The OD_{340} value was measured (the readout denoted as A1) at time of first reading (i.e. T1). OD_{34} was measured again (the readout denoted as A2) at time of second reading (i.e. T2 from 2 to 35 min). The amount of NADPH depletion (B) from T1 to T2 was evaluated as follows:

$$B = \frac{\Delta A_{340} - Intercept\ of\ NADPH\ standard\ curve}{Slope\ of\ NADPH\ standard\ curve}$$

Where $\Delta A_{340} = \frac{Sample\ A1 - Sample\ A2}{Control\ A1 - Control\ A2}$

The activity of GPx in the samples was expressed as nmol/min/mL= mU/mL and calculated as:

$$GPx\ activity = \left[\frac{B}{(T1 - T2) \times V}\right] \times D$$

Where V is the pretreated sample volume added to the reaction well (in mL); D is the dilution factor in the samples. Three replicates per condition were used to assess the average activity of GPx.

2.12. Analysis of Angiogenetic Potential of MSCs Using the Chick Chorioallantoic Membrane

Fertilized chicken eggs (HY-Line W-36) were obtained from the University of Illinois Poultry Farm (Urbana, IL). The eggs were incubated at 37 °C under humidity of 5% CO_2 atmosphere for 12 days. Following the initial incubation, a small window (approximately 1.5 cm diameter) was created on the egg shell to expose the chick chorioallantoic membrane (CAM). MSCs seeded in the collagen gel were incubated in media containing 200 μM H_2O_2

for 2 h before implanting onto the CAM. Conditions are as follows: (Group 1) collagen gel without cells, (Group 2) the collagen gel with untethered cells, (Group 3) the collagen gel with cells tethered with particles containing EGCG only, and (Group 4) the collagen gel with cells tethered with the H_2O_2-responsive anti-oxidizing particles. The window was then resealed with adhesive tapes and the eggs were returned to the incubator. After 6 days, the CAM was fixed with formalin for 24 h before excising the membrane. The excised CAM was subsequently embedded in paraffin and the cross-sections were stained for α-smooth muscle actin with diaminobenzidine (DAB) as peroxidase substrate. The immunostained samples were visualized with the NanoZoomer slide scanner (Hamamatsu, Japan) amplified using the NanoZoomer Digital Pathology (NDP) view software. The number of blood vessels and their individual cross-sectional area were manually quantified from six to seven different regions of CAM per condition.

2.13. Statistical Analysis

All data are expressed as mean ± standard deviation. Statistical analysis between two experimental groups was performed by the Student's t-test. A value of $p < 0.05$ indicated a statistically significant difference.

3. Results

3.1. Synthesis of PLGA-*b*-HA and Physical Characterization of PLGA-*b*-HA Particles Containing EGCG and MnO_2 Nanocatalysts

Block copolymer of PLGA-*b*-HA was synthesized using an end-to-end coupling between the carboxylate group of PLGA and an amino group of amine-functionalized HA [23]. The amphiphilicity of the purified PLGA-*b*-HA block copolymer was demonstrated by dissolving the block copolymers in deuterated water or deuterated DMSO and examining the ^{1}H NMR spectra (Figure S1). The characteristic peaks of the PLGA block were observed at 5.21, 4.91 and 1.47 in the organic solvent. In deuterated water, however, these peaks became broader due to restricted molecular movement of the protons on the PLGA block. Also, the peaks of the HA block at 3.36 – 4.60 ppm became more pronounced in the deuterated water than in the deuterated DMSO.

PLGA-*b*-HA particles encapsulating EGCG and MnO_2 nanocatalysts, termed as H_2O_2-responsive anti-oxidizing particles, were fabricated *via* the double emulsification. An aqueous mixture of EGCG and MnO_2 nanocatalysts was introduced to a mixture of dimethylformamide and dichloromethane dissolved with PLGA-*b*-HA. The emulsion was then transferred to another aqueous phase to yield the second emulsion. The presence of MnO_2 nanocatalysts in the PLGA-*b*-HA particles was confirmed with the transmission electron microscopic (TEM) images (Figure 2a). Particles with MnO_2 nanocatalysts (Figure 2a-ii) appeared darker and denser than the particles without MnO_2 nanocatalysts (Figure 2a–i). The average diameter of the resulting particles was 70 ± 10 nm as determined from the TEM images (Figure 2a-iii). With the double emulsification fabrication method, the encapsulation efficiency of the EGCG molecules and MnO_2 nanocatalysts was 74% and 10%, respectively.

In phosphate buffer saline, both particles with and without the MnO_2 nanocatalysts displayed a similar release profile (Figure 2b–i). We further examined the ability of particles to release EGCG in response to an elevated H_2O_2 level by incubating the particles in 200 μM H_2O_2 solution. The release rate of EGCG was quantified by measuring the mass of EGCG in the release medium at the designated time points and taking ratio with respect to the total mass of EGCG in the particles. By the first hour, the release rate of EGCG was 1.5-fold faster with the presence of MnO_2 nanocatalysts in the particles (Figure 2b-ii). The particles loaded with MnO_2 nanocatalysts released 100% of EGCG within 24 h. In contrast, particles without MnO_2 nanocatalysts released about 80% of the encapsulated EGCG. The release profile was similar to those of particles incubated in media free of H_2O_2.

In parallel, we monitored the rate of change in the H_2O_2 concentration in media containing free MnO_2 nanocatalysts, and the PLGA-*b*-HA particles with and without the MnO_2 nanocatalysts (Figure 2c). The concentration of H_2O_2 in the media was measured using a colorimetric assay kit that quantifies the amount of purple product formed from the complexation reaction between Fe^{3+} and the xylene orange provided. The concentration of Fe^{3+}, which is produced from the redox reaction between from Fe^{2+} and H_2O_2, is proportional to the concentration of H_2O_2. The decrease in the concentration of H_2O_2 from 200 μM was 1.5-fold faster in particles with MnO_2 nanocatalysts than those without the nanocatalysts within the first 2 h (Figure 2c). This decrement in the H_2O_2 concentration between the two groups became 2.3-fold at 24 h (Figure 2c). We presumed that all consumed H_2O_2 molecules were reacted into water and O_2 gas as follows:

$$2H_2O_2 \rightarrow 2H_2O + O_2$$

Using Figure 2c, we then calculated the increase in internal pressure of particles due to O_2 generation (ΔPO_2) at 24 h. With the stochiometric ratio between the number of moles of H_2O_2 and O_2 gas, we obtained the pressure of $O_2\left(P_{O_2}\right)$ through the equation of state for real gas:

$$P_{O_2} = \frac{z n_{O_2} RT}{V_{O_2}}$$

Where z is the compressibility factor of O_2 gas, n_{O_2} is the number of moles of O_2 generated, V_{O_2} is the volume of O_2 gas equivalent to the total volume of particles made from 10 mg of PLGA-*b*-HA polymer, R is the universal gas constant (8.314 $Jmol^{-1}K^{-1}$) and T is the working temperature at 310 K. Approximating the density of PLGA-*b*-HA polymer to be 1.3 g/mL, V_{O_2} was calculated to be 7.46×10^{-9} m^3.

The increase in O_2 pressure in the particles $\left(\Delta P_{O_2}\right)$ was eventually obtained by taking the difference between the total pressure of O_2 within the particles and the pressure of O_2

dissolved in the surrounding aqueous media. The detailed calculations are provided in the Supplementary Materials (Eq. 1 to Eq. 3) with the values of ΔP_{O_2} tabulated in Table S1. ΔP_{O_2} at 24 h was 8-fold higher for particles containing MnO_2 nanocatalysts (20.3 kPa) than that without the MnO_2 nanocatalysts (2.5 kPa) (Figure 2d).

3.2. Enhanced Surface Tethering to Stem Cells with PLGA-*b*-HA Particles

Surface tethering of mesenchymal stem cells with the particles was achieved through HA-CD44 interactions. To assess the importance of the HA blocks in surface tethering, we labelled particles with and without the HA blocks by loading bovine serum albumin conjugated with Rhodamine B (Figure 3a). Immediately after mixing the stem cells with these particles and removing unbound particles through centrifugation, we observed a higher red intensity on the surface of cells (green) tethered with PLGA-*b*-HA particles (Figures 3b and S3a). The equilibrium duration for the tethering process was evaluated by measuring the fluorescence intensity of Rhodamine B in the supernatant after centrifugation. It took approximately 15 min for the largest number of particles to anchor to the stem cells (Figure S2).

Interestingly, we observed that the PLGA-*b*-HA particles (red) bound to the cell membrane (green) in clusters of size as large as 1 μm (Figures 3b and S3a). These aggregates could prevent the likelihood of being taken up by the cells as the upper size limit for cellular internalization by non-phagocytic cells is < 1 μm [25]. After 24 h of incubation, a certain fraction of particles was within the cell body due to cellular uptake (Figure S3b). After 72 h, a minimal number of particles was found, likely due to hydrolytic degradation of particles (Figure S3c) [26,27].

In parallel, we determined the binding kinetics of the particles to the surface of cells by measuring the association and dissociation rates. The experimental setup (Schematic S1 in Supplementary Materials) and derivations of the binding kinetics are provided in the Supplementary Materials (Eq. 4 to Eq. 6). Assuming a bimolecular reversible interaction between the particles and cells, PLGA-*b*-HA particles exhibited 3.6-fold higher association rate to cells and 4.4-fold lower dissociation rate from cells than PLGA particles. Therefore, the binding affinity of PLGA-*b*-HA particles to stem cells was 20-fold higher than PLGA particles.

Since injection, be it intravenous or local, is the primary technique of delivering these surface tethered cells, we evaluated the likelihood of particles retaining on the surface of cells following injection. A suspension of cells tethered with fluorescently-labeled PLGA-*b*-HA particles was pushed through a needle (26G, ½ inch) using a syringe pump. With an injection speed of 1.5 mL/min, 37 ± 1% of the particles were detached.

3.3. H_2O_2-Responsive Anti-Oxidizing Particles Serve to Retain Metabolic Activity and Morphology of Stem Cells in an Oxidative Environment

We next examined the metabolic activity of stem cells in an H_2O_2-rich environment. Stem cells were tethered with EGCG-loaded PLGA-*b*-HA particles with and without MnO_2

nanocatalysts and seeded in the collagen gel (Figure 4a). We then exposed the stem cells to H_2O_2 solution of 100 μM and 200 μM for 2 h (Figure 4a). This condition stimulates stem cells transplanted to treat acute injury such as cutaneous wounding and ischemic injury [28]. After 2h, cells were cultured in the media free of H_2O_2. The metabolically active cells were identified with positive staining by the 2,3-Bis-(2-Methoxy-4-Nitro-5-Sulfophenyl)-2H-Tetrazolium-5-Carboxanilide (XTT) assay. The overall level of metabolic activity of each group was expressed as a percentage of the absorbance values of the control groups not exposed to H_2O_2. Stem cells tethered with H_2O_2-responsive anti-oxidizing particles displayed a 1.1-fold higher metabolic activity than untethered cells following 2 h exposure to 100 μM of H_2O_2 (Figure S4a). The protective efficacy of these particles became more significant when H_2O_2 level was increased to 200 μM. Specifically, the overall metabolic activity per initial number of cells seeded was higher at 1.2-fold and 1.6-fold than cells tethered with particles loading EGCG only and untethered cells, respectively (Figure 4b). Additionally, they retained their protective capability in 200 μM H_2O_2 following lyophilization and storage over 4 weeks, suggesting that EGCG and MnO_2 nanocatalysts remained stable. In contrast, the H_2O_2-responsive anti-oxidizing particles could not salvage stem cells exposed to H_2O_2 solution (50 μM and 100 μM) for 16 h, which simulates the chronically oxidative environment (Figure S4b). Lower concentrations of H_2O_2 at 50 μM and 100 μM were examined as there is a notion that chronic H_2O_2 level is lower than the H_2O_2 level resulting from acute injuries [29]. Moreover, the approach of tethering the stem cells with H_2O_2-repsonsive anti-oxidizing particles did not induce observable change to the metabolic activity of the cells. No significant difference in the overall cell metabolic activity was observed between cells tethered with the H_2O_2-responsive anti-oxidizing particles and untethered cells at 2 h, on Day 1 and Day 4 after mixing (Figure S4c).

In parallel, we assessed the morphology of the cells in the various experimental groups on Day 4 by capturing 2D projected images of the cells using an optical microscope (Figure S5). We then quantified the cell shape index (CSI) [30] as follows:

$$Cell\ shape\ index = \frac{4\pi A}{P^2}$$

Where A is the area of the cell (μm^2) and P is the perimeter of the cell (μm).

A dimensionless parameter, the CSI measures the circularity of a cell. Using ImageJ, we traced the periphery individual cells to obtain the respective cell area and perimeter. We then quantified the inverse of CSI values. On Day 4 following 2 h exposure to 200 μM H_2O_2, cells tethered with H_2O_2-responsive anti-oxidizing particles exhibited approximately 2-fold and 5-fold higher reduced roundness than cells tethered with particles loading EGCG only and untethered cell, respectively (Figure 4c). In contrast, cells unexposed to H_2O_2 displayed comparable cell spreading across all experimental groups (Figure 4c).

3.4. H_2O_2-Responsive Anti-oxidizing Particles Retain Proangiogenic Factor-Secretion Activity of Stem Cells in an Oxidative Environment

We then evaluated the secretory activity of the stem cells in an oxidative environment by measuring the concentration of vascular endothelial growth factor (VEGF) in the conditioned media (Figure 5a). Stem cells cultured in the H_2O_2-free media secreted comparable levels of VEGF across all conditions on Day 1 and Day 4 (Figure 5b). Cells in all conditions displayed the increased VEGF secretion level.

Alternatively, cells were exposed to media containing 200 μM H_2O_2 for 2 h. Then, cells were cultured in the media free of H_2O_2 for 1 day or 4 days. Both the untethered stem cells and those tethered with blank particles secreted 3-fold and 60-fold lower VEGF levels on Day 1 and Day 4, respectively, than those cultured in the H_2O_2-free media (Figure 5b). Additionally, these two groups undertook a drastic decrease in the secretion level of VEGF by 4-fold throughout 4 days of cell culture (Figure 5b). On the contrary, on Day 1, cells tethered with particles loading EGCG and MnO_2 nanocatalysts secreted 1.4-fold higher mass of VEGF than those tethered with particles without MnO_2 nanocatalysts (Figure 5b). This difference between the two conditions became more significant on Day 4 by a fold-change of 5 (Figure 5b). Furthermore, stem cells tethered with particles loading EGCG only exhibited a VEGF secretion level comparable to the untethered cells and those tethered with blank particles.

3.5. H_2O_2-Responsive Anti-oxidizing Particles Tethered to Cells Reduce Intracellular Oxidative Stress and Enhance Activity of Glutathione Peroxidase

We studied the mechanism by which the particles loading EGCG and MnO_2 nanocatalysts reduced the impacts of H_2O_2 on stem cells by analyzing the intracellular oxidative stress level and the antioxidant enzyme glutathione peroxidase (GPx) activity. The intracellular oxidative stress level was examined with CellROX® Green which emits green fluorescence upon reactive oxygen species-induced oxidation and subsequently binds to DNA. The average intensity of the CellROX® Green in each cell was measured by first converting the fluorescence images into grayscale images. Then, we quantified the mean gray value of the CellROX® Green, which indicates the brightness of a pixel. Cells incubated in the media containing 200 μM H_2O_2 for 2 h increased the intensity of CellROX® Green (Figures 6a and 6b). On the other hand, cells tethered with particles loading EGCG only decreased the positive green fluorescence by 1.5-fold, as compared with the untethered cells. Furthermore, stem cells tethered with particles loading EGCG and MnO_2 nanocatalysts displayed 3-fold decrease in the intensity (Figures 6a and 6b). A z-stack sweep-through of the CellROX® Green in an individual untethered cell (Movie S1a), a cell tethered with particles loading EGCG only (Movie S1b), and a cell tethered with particles loading EGCG and MnO_2 nanocatalysts (Movie S1c) is provided in the Supplementary Materials.

The activity of GPx in stem cells was assessed following exposure to either culture media or media containing 200 μM H_2O_2 for 2 h. The GPx level was measured by quantifying the depletion rate of dihydronicotinamide-adenine dinucleotide phosphate (NADPH) during the redox reaction of glutathione. To ensure that the value of GPx activity is independent of the fraction of metabolically active cells, we normalized it with respect to the number of

metabolically active cells in each condition. Untethered stem cells displayed a similar GPx activity level in both H_2O_2-free media and 200 μM H_2O_2-containing media (Figure 6c). On the contrary, in the H_2O_2-containing media, cells tethered with particles loading EGCG only and those tethered with particles loading EGCG and MnO_2 nanocatalysts showed a 1.3-fold higher GPx level than untethered stem cells and those tethered with blank particles (Figure 6c). Cells tethered with particles loading MnO_2 nanocatalysts only exhibited comparable GPx activity with the untethered cells and those with the blank particles.

3.6. H_2O_2-Responsive Anti-Oxidizing Particles Tethered to Cells Enhance Neovascularization

Finally, we examined the extent to which the H_2O_2-responsive anti-oxidizing particles improved the angiogenic potential of H_2O_2-exposed stem cells using the chick chorioallantoic membrane (CAM). Collagen gels encapsulating stem cells were embedded onto the membrane and incubated over 6 days before analyzing mature vasculature formed at the site implanted with the collagen gel (Figure 7a). The mature blood vessels in the CAM were identified with positive staining of α-smooth muscle actin (red arrows in Figure 7b). Control conditions included the cell-free collagen gel, the collagen gel encapsulating untethered stem cells, and the collagen gel encapsulating stem cells tethered with particles loading EGCG only. Compared with these three conditions, collagen gels encapsulating stem cells tethered with particles loading EGCG and MnO_2 nanocatalysts doubled the number α-smooth muscle actin-positive blood vessels. Approximately 40% of the vessels had the cross-sectional area larger than 500 μm^2 (Figures 7c and 7d). On the contrary, the majority of blood vessels in CAM implanted with the collagen gel containing with and without stem cells had cross-sectional areas between 50–200 μm^2 (i.e. ~50–60% of total number of blood vessels). Stem cells tethered with particles loading EGCG only yielded blood vessels with intermediate cross-sectional areas of 200–500 μm^2.

4. Discussion

The results of this study have successfully demonstrated an approach that protects mesenchymal stem cells from H_2O_2-induced death and subsequently maintains their metabolic activity and angiogenic potential. This approach encompasses the tethering of stem cells with PLGA-*b*-HA particles that can release epigallocatechin gallate (EGCG), a model anti-oxidant, in response to elevated levels of H_2O_2. We exploited the fact that mesenchymal stem cells express HA-binding CD44 receptors on their surface [31,32]. To leverage on these receptors, we conjugated HA blocks to the PLGA blocks. Additionally, HA contributes to increasing the hydrophilicity of the particle surface. PLGA, which serves as the hydrophobic component of the copolymer, can undergo hydrolytic degradation in physiological fluids [26,33].

These particles, termed as H_2O_2-responsive anti-oxidizing particles, were loaded with EGCG and Manganese (IV) oxide (MnO_2) nanocatalysts through the double emulsification process. During the second emulsification, a larger volume of the aqueous surfactant solution could drive some of the hydrophobic PLGA blocks to reorient themselves inward,

and the corresponding HA blocks would now be facing the aqueous surrounding, giving rise to a putative bilayer (Schematic S2 in Supplementary Materials).

This bilayer could slow the diffusion of solute molecules into the particles compared to monolayered particles fabricated through single emulsification process. However, since H_2O_2 molecules are very small (0.25–0.28 nm) [34], diffusion of H_2O_2 through the bilayer is not likely to pose a significant problem. Rather, hydrophilic HA blocks of PLGA-*b*-HA would facilitate diffusion of H_2O_2 into particles compared with hydrophobic PLGA particles. Accordingly, the PLGA-*b*-HA particles would be advantageous to induce catalytic H_2O_2 decomposition reaction compared with PLGA particles. This insight would be examined systematically in future studies.

The H_2O_2-responsive anti-oxidizing particles displayed the accelerated release rate of EGCG exclusively in the presence of H_2O_2. On the other hand, the release rate of EGCG from particles without the MnO_2 nanocatalysts did not show dependency on the H_2O_2 level.

We propose that the H_2O_2-responsive release of EGCG results from the O_2 generation caused by the rapid decomposition of H_2O_2. When the H_2O_2-responsive anti-oxidizing particles were exposed to H_2O_2, H_2O_2 molecules would diffuse into the particles. The MnO_2 nanocatalysts encapsulated in the particles would subsequently catalyze the decomposition of these H_2O_2 molecules. This H_2O_2 decomposition may proceed through a series of chain reactions involving redox couple Mn^{4+}/Mn^{3+} and the formation of radical HO_2• that propagates the conversion of H_2O_2 into water and O_2 gas [35]. The introduction of O_2 gas in the particles would then increase the internal pressure of the particles. The resulting increase in the pressure difference between inside and outside of particles acts as a pump that drives the release of the encapsulated EGCG cargos [22]. Amongst the numerous metal oxides, manganese (IV) oxide was chosen as it demonstrates the highest reactivity in promoting the decomposition of H_2O_2 and thus, generating the largest amount of O_2 gas within a given period [36]. In this study, we assessed the protective function of the particles using media containing 200 μM H_2O_2. This H_2O_2 concentration falls within the pathophysiological relevant levels of H_2O_2 in ischemia [37,38].

The highlight of this study also lies in the approach to tether the H_2O_2-responsive anti-oxidizing particles to stem cells and, in turn, to retain the therapeutic potential of stem cells in a harsh oxidative environment *in situ*. The air temperature in the operating room is typically recommended to be kept between 20–23 °C [39]. To simulate the process of modifying cell surface with the H_2O_2-responsive anti-oxidizing particles in the operation room for cell transplantation, we tethered the stem cells with PLGA-*b*-HA particles in suspension at ambient conditions. By measuring the fluorescence intensity of Rhodamine B in the particles, we determined that it took approximately 15 minutes for the particles to adhere to cell surface. Since HA binds specifically with CD44 [40], we propose that the increased binding affinity of the PLGA-*b*-HA particles to cells was due to the HA-CD44 interactions between the particles and the cells, which were not available to the PLGA particles. In addition, the limited attachment of PLGA particles on the stem cell surface shown on the confocal images further confirms the critical role of HA-CD44 interactions for the cell surface tethering.

We determined the dose of the H_2O_2-responsive anti-oxidizing particles based on the final amount of EGCG encapsulated in the particles. The dose of EGCG was selected such that it did not exceed the toxic limit to mammalian cells but sufficiently high to bring about the protective effects in an oxidative environment (i.e. increased GPx activity). Depending on the types of cell line, *in vitro* toxicity of EGCG occurs at a concentration of 100 μM with human lymphocytes [41,42] or 440 μM with human gingival fibroblasts [43]. Separately, EGCG at a minimal concentration of 2.5 μM was enough to achieve a 2.8-fold increment in the activity of GPx in MSCs exposed to H_2O_2 [19]. Thus, the dose of EGCG in the H_2O_2-repsonsive anti-oxidizing particles was selected to lie around 2.5 μM but less than 100 μM. The calculated dose of EGCG in the H_2O_2-repsonsive anti-oxidizing particles was about 3.5 μM, which fits within the selected range.

The resulting H_2O_2-responsive anti-oxidizing particles tethered to cells could successfully protect cells from the H_2O_2. We purposely seeded stem cells in a collagen gel to mimic the tissue microenvironment where the stem cells are transplanted. The H_2O_2-responsive anti-oxidizing particles improved the metabolic activity of cells by 1.2-fold as compared to particles loading EGCG only, due to the enhanced release of EGCG within the first 2 h. By Day 4, the protective role of these H_2O_2-responsive anti-oxidizing particles became more significant with a 1.3-fold higher metabolic activity than that of the particles loading EGCG only. Correspondingly, these cells exhibited a larger extent of spreading than those tethered with particles loading EGCG only, as reflected by the 2-fold higher in the inverse of cell shape index.

Although the media containing H_2O_2 was replaced with the H_2O_2-free cell culture media after 2 h, it is likely that cells could not recover from the oxidative damage, thus failing to proliferate thereafter. Additionally, we suggest that the elevated internal pressure of the anti-oxidizing particles did not revert immediately and sustained the increased release of EGCG. Therefore, it is highly likely that cells tethered with the H_2O_2-responsive anti-oxidizing particles could produce daughter cells through continued cell division, thereby amplifying the differences in the number of metabolically active cells between conditions over days.

This study also presents a positive correlation between the metabolic activity and proangiogenic factor secretion activity of stem cells. Since mesenchymal stem cells secrete soluble VEGF [44–46], the concentration of this growth factor in the cell culture media would concur with the level of cellular secretion. On Day 1 and Day 4 after exposure to the H_2O_2 solution, stem cells tethered with the H_2O_2-responsive anti-oxidizing particles exhibited higher metabolic activity and VEGF secretion levels than control conditions. These controls include the untethered stem cells, stem cells tethered with blank particles, and stem cells tethered with particles loading EGCG only. Intriguingly, the metabolic activity of both untethered stem cells and stem cells tethered with blank particles did increase over the next three days. However, their secretion activity plummeted instead. Such results suggest that cells, although appeared to be metabolically active, were not in the conducive state to secrete the pro-angiogenic factor. In contrast, cells identified to be metabolically active for those tethered with the H_2O_2-responsive anti-oxidizing particles likely remained active to secrete VEGF in an oxidative environment. We propose that the cells tethered with the H_2O_2-responsive anti-oxidizing particles would also be active to

secrete various anti-apoptotic and immunomodulatory factors [2–5,47]. This perspective will be examined systematically in future studies.

The entry of H_2O_2 into stem cells and subsequent accumulation would raise the intracellular oxidative stress level. Accordingly, untethered stem cells experienced an elevated oxidative stress level following the exposure to H_2O_2 for 2 h, as reflected by the strong green fluorescence intensity of CellROX® Green. CellROX® Green remains non-fluorescent until it gets oxidized by reactive oxygen species (e.g. H_2O_2) in the cells. Therefore, the fluorescence intensity of CellROX® Green is proportional to the level oxidative stress. In contrast, stem cells tethered with particles loading EGCG only and those tethered with the H_2O_2-responsive anti-oxidizing particles showed limited increase in the oxidative stress. We attributed this observation to the improved activity of the antioxidant enzyme, GPx, in the cells.

In an oxidative intracellular environment, GPx catalyzes the reduction of H_2O_2 to water while oxidizing reduced monomeric glutathione (GSH) to glutathione disulfide (GSSG) in Reaction (1) [48].

$$2GSH + H_2O_2 \xrightarrow{GPx} GSSG + 2H_2O \quad \text{Reaction (1)}$$

With a higher activity of GPx per metabolically active cell, more H_2O_2 molecules in the cells get depleted and, in turn, reduce the level of intracellular oxidative stress. EGCG molecules released from the particles stimulated the activity of GPx in stem cells exposed to H_2O_2. Interestingly, however, the activity of GPx did not differ significantly between the particles loading EGCG and MnO_2 nanocatalysts and those encapsulating EGCG only. Additionally, particles loading MnO_2 nanocatalysts only were not effective to increase the activity of GPx although they suppressed the increase of the intracellular oxidative stress. Taken together, we propose that the MnO_2 nanocatalysts in the particles depleted the H_2O_2 surrounding the cells such that a smaller number of H_2O_2 molecules entered and accumulated in the cells. These mechanistic studies implicate a collaborative effort between the EGCG molecules and the MnO_2 nanocatalysts in improving cellular survival and retaining the therapeutic potential of cells in an oxidative environment.

The positive correlation between cellular metabolic activity and secretion activity of proangiogenic factors established *in vitro* was also observed *in vivo*. CAM implanted with the collagen gel encapsulating stem cells tethered with H_2O_2-responsive anti-oxidizing particles exhibited the largest number of mature blood vessels on Day 6-post implantation. The enhanced cellular metabolic activity led to an increased collective amount of VEGF secreted by the stem cells. This, in turn, stimulated the growth of new blood vessels and the maturity of existing vessels, as reflected by the formation of blood vessels with cross-sectional areas of over 500 μm^2. In contrast, the lower metabolic activity and VEGF secretion levels of untethered stem cells and stem cells tethered with blank particles yielded the limited increases in the number and size of blood vessels in CAMs.

Our study adopted a 2 h exposure of stem cells to H_2O_2 solution to assess the protective effect of the H_2O_2-responsive anti-oxidizing particles. This condition simulates acute injuries where the increase in H_2O_2 level is transient [28]. Also, the impacts of H_2O_2 on cells were observed even several days later. Untethered cells exhibited the lowest overall metabolic activity and secreted the least amount of VEGF on Day 4 following the 2 h exposure to H_2O_2. On the other hand, H_2O_2-responsive anti-oxidizing particles tethered to cells increased the number of metabolically active cells by 1.4-fold on Day 4. These particles also maintained the angiogenic potential of the cells to stimulate formation of microvascular networks *in vivo* through six days. Therefore, we propose that tethering the stem cells with these H_2O_2-responsive anti-oxidizing particles would be advantageous to restoring metabolic activity and therapeutic potential of cells damaged by acute exposure to H_2O_2.

To the best of our knowledge, this is the first report on tethering the cellular surface with H_2O_2-responsive anti-oxidizing particles for retaining the therapeutic potential of stem cells in an oxidative environment. Previous efforts have focused on increasing the resilience of stem cells against oxidative stress by transfecting them with anti-apoptotic genes of the protein kinase B (AKT) [49] or heat shock proteins including Hsp-20 [50]. Pretreatment of stem cells with a cocktail of antioxidants in culture media before transplantation is another strategy [18]. In contrast, our non-genetic approach improves the intrinsic anti-oxidizing activity of stem cells and, at the same time, reduces the H_2O_2 level at the transplanted sites. More importantly, the short process of tethering stem cells with the H_2O_2-responsive anti-oxidizing particles does not necessitate the exposure of cells to culture media containing xenogeneic products and it can be performed right before cell transplantation.

5. Conclusions

This study presented an approach to protect therapeutic stem cells and to maintain their secretion activity in an oxidative environment. PLGA-*b*-HA particles containing antioxidant EGCG and MnO_2 nanocatalysts, named as H_2O_2-responsive anti-oxidizing particles, were tethered onto the surface of stem cells *via* HA-CD44 interactions. When exposed to sub-lethal physiopathologically relevant concentration of H_2O_2, a majority of cells tethered with the H_2O_2-responsive anti-oxidizing particles remained active to secrete proangiogenic factors. The intracellular oxidative stress in the stem cells also declined to a level comparable to those without H_2O_2 exposure. Mechanistic studies disclosed that MnO_2 nanocatalysts in the particles reduced the concentration of H_2O_2 by decomposing it to O_2 gas, which in turn accelerated the release of the encapsulated EGCG. The released EGCG improved the activity of antioxidizing enzyme glutathione peroxidase. Consequently, the H_2O_2-responsive anti-oxidizing particles tethered to stem cells increased the cellular secretion of pro-angiogenic VEGF and in turn, the number of newly formed mature blood vessels. Therefore, the results in this study will broadly serve to improve the therapeutic potential of a wide array of stem cells.

Supplementary Material

Refer to Web version on PubMed Central for supplementary material.

Acknowledgements

This work was supported by the National Institutes of Health (Grant 1R01 HL109192 and 1 R21 HL131469 to H. Kong) and National Science Foundation (CBET-1403491 to H. Kong). J.Y. Teo and J. Leong acknowledge the support of A*STAR Graduate Scholarship (Overseas) from the Agency for Science, Technology, and Research (A*STAR), Singapore. E. Ko acknowledges the support from the National Institute of Biomedical Imaging and Bioengineering of the National Institutes of Health (Award T32EB019944). Y.Y. Yang acknowledges the support from the Institute of Bioengineering and Nanotechnology (Biomedical Research Council, Agency for Science, Technology, and Research), Singapore.

References

[1]. Phinney DG, Prockop DJ. Concise review: mesenchymal stem/multipotent stromal cells; the state of transdifferentiation and modes of tissue repair—current views, Stem Cells. 25 (2007) 2896–2902. 10.1634/stemcells.2007-0637. [PubMed: 17901396]

[2]. Nauta AJ, Willem EF. Immunomodulatory properties of mesenchymal stromal cells, Blood. 110 (2007) 3499–3506. 10.1182/blood-2007-02-069716. [PubMed: 17664353]

[3]. Kyurkchiev D, Bochev I, Ivanova-Todorova E, Mourdjeva M, Oreshkova T, Belemezova K, Kyurkchiev S. Secretion of immunoregulatory cytokines by mesenchymal stem cells, World J. Stem Cells. 6 (2014) 552–570. 10.4252/wjsc.v6.i5.552. [PubMed: 25426252]

[4]. Ma S, Xie N, Li W, Yuan B, Shi Y, Wang Y. Immunobiology of mesenchymal stem cells, Cell Death Differ. 21 (2014) 216–225. 10.1038/cdd.2013.158. [PubMed: 24185619]

[5]. Baraniak PR, McDevitt TC. Stem cell paracrine actions and tissue regeneration, Regen. Med 5 (2010) 121–143. 10.2217/rme.09.74. [PubMed: 20017699]

[6]. Nguyen PK, Riegler J, Wu JC. Stem cell imaging: from bench to bedside, Cell Stem Cell. 14 (2014) 431–444. 10.1016/j.stem.2014.03.009. [PubMed: 24702995]

[7]. Gyöngyösi M, Blanco J, Marian T, Trón L, Petneházy O, Petrasi Z, Hemetsberger R, Rodriguez J, Font G, Pavo IJ, Kertész I, Balkay L, Pavo N, Posa A, Emri M, Galuska L, Kraitchman DL, Wojta J, Huber K, Glogar D. Serial noninvasive in vivo positron emission tomographic tracking of percutaneously intramyocardially injected autologous porcine mesenchymal stem cells modified for transgene reporter gene expression. Circ. Cardiovasc. Imaging, 1 (2008) 94–103. 10.1161/CIRCIMAGING.108.797449. [PubMed: 19808526]

[8]. Hoffmann J, Glassford AJ, Doyle TC, Robbins RC, Schrepfer S, Pelletier MP. Angiogenic effects despite limited cell survival of bone marrow-derived mesenchymal stem cells under ischemia, Thorac. Cardiovasc. Surg 58 (2010) 136–142. 10.1055/s-0029-1240758. [PubMed: 20379963]

[9]. Solaini G, Baracca A, Lenaz G, Sgarbi G. Hypoxia and mitochondrial oxidative metabolism, Biochim. Biophys. Acta 1797 (2010) 1171–1177. 10.1016/j.bbabio.2010.02.011. [PubMed: 20153717]

[10]. Gao L, Laude K, Cai H. Mitochondrial pathophysiology, reactive oxygen species, and cardiovascular diseases, Vet. Clin. North Am. Small Anim. Pract 38 (2008) 137–iv. 10.1016/j.cvsm.2007.10.004. [PubMed: 18249246]

[11]. Guzy RD, Schumacker PT. Oxygen sensing by mitochondria at complex III: the paradox of increased reactive oxygen species during hypoxia, Exp. Physiol 91 (2006) 807–819. 10.1113/expphysiol.2006.033506. [PubMed: 16857720]

[12]. Nita M, Grzybowski A. The role of the reactive oxygen species and oxidative stress in the pathomechanism of the age-related ocular diseases and other pathologies of the anterior and posterior eye segments in adults, Oxid. Med. Cell. Longev 2016 (2016) 3164734 10.1155/2016/3164734.

[13]. Mackenzie EL, Iwasaki K, Tsuji Y. Intracellular iron transport and storage: from molecular mechanisms to health implications, Antioxid. Redox Signal 10 (2008) 997–1030. 10.1089/ars.2007.1893. [PubMed: 18327971]

[14]. Birben E, Sahiner UM, Sackesen C, Erzurum S, Kalayci O. Oxidative stress and antioxidant defense, World Allergy Organ. J 5 (2012) 9–19. 10.1097/WOX.0b013e3182439613. [PubMed: 23268465]

[15]. Lobo V, Patil A, Phatak A, Chandra N. Free radicals, antioxidants and functional foods: impact on human health, Pharmacogn. Rev 4 (2010) 118–126. 10.4103/0973-7847.70902. [PubMed: 22228951]

[16]. Bhattacharyya A, Chattopadhyay R, Mitra S, Crowe SE. Oxidative stress: an essential factor in the pathogenesis of gastrointestinal mucosal diseases, Physiol. Rev 94 (2014) 329–354. 10.1152/physrev.00040.2012. [PubMed: 24692350]

[17]. Wei H, Li Z, Hu S, Chen X, Cong X. Apoptosis of mesenchymal stem cells induced by hydrogen peroxide concerns both endoplasmic reticulum stress and mitochondrial death pathway through regulation of caspases, p38 and JNK, J. Cell Biochem 111 (2010) 967–978. 10.1002/jcb.22785. [PubMed: 20665666]

[18]. Schäfer R, Spohn G, Baer PC. Mesenchymal stem/stromal cells in regenerative medicine: can preconditioning strategies improve therapeutic efficacy? Transfus. Med. Hemother 43 (2016) 256–267. 10.1159/000447458. [PubMed: 27721701]

[19]. Yagi H, Tan J, Tuan RS. Polyphenols suppress hydrogen peroxide-induced oxidative stress in human bone-marrow derived mesenchymal stem cells, J. Cell Biochem 114 (2013) 1163–1173. 10.1002/jcb.24459. [PubMed: 23192437]

[20]. Mao X, Gu C, Chen D, Yu B, He J. Oxidative stress-induced diseases and tea polyphenols, Oncotarget. 8 (2017) 81649–81661. 10.18632/oncotarget.20887. [PubMed: 29113421]

[21]. Selvaggi TA, Walker RE, Fleisher TA. Development of antibodies to fetal calf serum with arthus-like reactions in human immunodeficiency virus-infected patients given syngeneic lymphocyte infusions, Blood. 89 (1997) 776–779. [PubMed: 9028307]

[22]. Seo Y, Leong J, Teo JY, Mitchell JW, Gillette MU, Han B, Lee J, Kong H. Active antioxidizing particles for on-demand pressure-driven molecular release, ACS Appl. Mater. Interfaces 9 (2017) 35642–35650. 10.1021/acsami.7b12297. [PubMed: 28961399]

[23]. Huang J, Zhang H, Yu Y, Chen Y, Wang D, Zhang G, Liu J, Sun Z, Sun D, Lu Y, Zhong Y. Biodegradable self-assembled nanoparticles of poly(D,L-lactide-co-glycolide)/hyaluronic acid block copolymers for target delivery of docetaxel to breast cancer, Biomaterials. 35 (2014) 550–566. 10.1016/j.biomaterials.2013.09.089. [PubMed: 24135268]

[24]. Liang Y, Jeong J, DeVolder RJ, Cha C, Wang F, Tong Y, Kong H. A cell-instructive hydrogel to regulate malignancy of 3D tumor spheroids with matrix rigidity, Biomaterials. 32 (2014) 9308–9315. 10.1016/j.biomaterials.2011.08.045.

[25]. Rejman J, Oberle V, Zuhorn IS, Hoekstra D. Size-dependent internalization of particles via the parthways of clathrin- and caveolae-mediated endocytosis, Biochem. J 337 (2004) 159–169. 10.1042/bj20031253.

[26]. Makadia HK, Siegel SJ. Poly Lactic-co-Glycolic Acid (PLGA) as Biodegradable Controlled Drug Delivery Carrier, Polymers (Basel). 3 (2011) 1377–1397. 10.3390/polym3031377. [PubMed: 22577513]

[27]. Tokita Y, Okamoto A. Hydrolytic degradation of hyaluronic acid, Polym. Degrad. Stab 48 (1995) 269–273. 10.1016/0141-3910(95)00041-J.

[28]. Gauron C, Rampon C, Bouzaffour M, Ipendey E, Teillon J, Volovitch M, Vriz S. Sustained production of ROS triggers compensatory proliferation and is required for regeneration to proceed, Sci. Rep 3 (2013) 2084 10.1038/srep02084. [PubMed: 23803955]

[29]. Roy S, Khanna S, Nallu K, Hunt TK. Dermal wound healing is subject to redox control, Mol. Ther 13 (2005) 211–220. 10.1016/j.ymthe.2005.07.684 [PubMed: 16126008]

[30]. Choi JS, Harley BAC. The combined influence of substrate elasticity and ligand density on the viability and biophysical properties of hematopoietic stem and progenitor cells, Biomaterials. 33 (2012) 4460–4468. 10.1016/j.biomaterials.2012.03.010 [PubMed: 22444641]

[31]. Gimble JM, Katz AJ, Bunnell BA. Adipose-derived stem cells for regenerative medicine, Circ. Res 100 (2007) 1249–1260. 10.1161/01.RES.0000265074.83288.09. [PubMed: 17495232]

[32]. Mildmay-White A, Khan W. Cell surface markers on adipose-derived stem cells: a systemic review, Curr. Stem. Cell. Res. Ther 12 (2017) 484–492. 10.2174/1574888X11666160429122133. [PubMed: 27133085]

[33]. Lü JM, Wang X, Marin-Muller C, Wang H, Lin PH, Yao Q, Chen C. Current advances in research and clinical applications of PLGA-based nanotechnology, Expert. Rev. Mol. Diagn 9 (2009) 325–341. 10.1586/erm.09.15 [PubMed: 19435455]

[34]. Bienert GP, Schjoerring JK, Jahn TP. Membrane transport of hydrogen peroxide, Biochim. Biophys. Acta 1758 (2006) 994–1003. 10.1016/j.bbamem.2006.02.015. [PubMed: 16566894]

[35]. Sorge AR, Turco M, Pilone G, Bagnasco G. Decomposition of hydrogen peroxide on MnO_2/TiO_2 catalysts, J Propul Power. 20 (2004) 1069–1075. 10.2514/1.2490.

[36]. Russo V, Protasova L, Turco R, de Croon MHJM, Hessel V, Santacesaria E. Hydrogen peroxide decomposition on manganese oxide supported catalyst: from batch reactor to continuous microreactor, Ind. Eng. Chem. Res 52 (2013). 7668–7676. 10.1021/ie303543x.

[37]. Coombes E, Jiang J, Chu XP, Inoue K, Seeds J, Branigan D, Simon RP, Xiong ZG. Pathophysiologically relevant levels of hydrogen peroxide induce glutamate-independent neurodegeneration that involves activation of transient receptor potential melastatin 7 channels, Antioxid. Redox Signal 14 (2011) 1815–1827. 10.1089/ars.2010.3549. [PubMed: 20812867]

[38]. Oshikawa J, Urao N, Kim HW, Kaplan N, Razvi M, McKinney R, Poole LB, Fukai T, Ushio-Fukai M. Extracellular SOD-derived H2O2 promotes VEGF signaling in caveolae/lipid rafts and post-ischemic angiogenesis in mice, PLoS One. 5 (2010) e10189 10.1371/journal.pone.0010189. [PubMed: 20422004]

[39]. Blanchard J. Humidity, temperature, and air exchanges in the OR, AORN J. 89 (2009) 1129–1131. 10.1016/j.aorn.2009.05.012.

[40]. Lesley J, Hascall VC, Tammi M, Hyman R. Hyaluronan Binding by Cell Surface CD44. J Biol Chem 2000, 275, 26967–26975. 10.1074/jbc.M002527200. [PubMed: 10871609]

[41]. Nance CL, Siwak EB, Shearer WT. Preclinical development of the green tea catechin, epigallocatechin gallate, as an HIV-1 therapy, J. Allery Clin. Immunol 123 (2009) 459–465. 10.1016/j.jaci.2008.12.024.

[42]. Elbling L, Weiss RM, Teufelhofer O, Uhl M, Knasmueller S, Schulte-Hermann R, Berger W, Micksche M. Green tea extract and (−)-epigallocatechin-3-gallate, the major tea catechin, exert oxidant but lack antioxidant activities, FASEB J. 19 (2005) 807–809. 10.1096/fj.04-2915fje. [PubMed: 15738004]

[43]. Weisburg JH, Weissman DB, Sedaghat T, Babich H. In vitro cytotoxicity of epigallocatechin gallate and tea extracts to cancerous and normal cells from the human oral cavity, Basic Clin. Pharmacol. Toxicol 95 (2004) 191–200. 10.1111/j.1742-7843.2004.pto_950407.x. [PubMed: 15504155]

[44]. Salgado AJ, Reis RL, Sousa NJ, Gimble JM. Adipose tissue derived stem cells secretome: soluble factors and their roles in regenerative medicine, Curr. Stem Cell Res. Ther 5 (2010) 103–110. 10.2174/157488810791268564. [PubMed: 19941460]

[45]. Meirelles Lda S, Fontes AM, Covas DT, Caplan AI. Mechanisms involved in the therapeutic properties of mesenchymal stem cells, Cytokine Growth Factor Rev. 20 (2009) 419–427. 10.1016/j.cytogfr.2009. [PubMed: 19926330]

[46]. Saldaña L, Vallés GG, Bensiamar F, Mancebo FJ, García-Rey E, Vilaboa N. Paracrine interactions between mesenchymal stem cells and macrophages are regulated by 1,25-dihydroxyvitamin D3, Sci. Rep 7 (2017) 14618 10.1038/s41598-017-15217-8. [PubMed: 29097745]

[47]. Rehman J, Traktuev D, Li J, Merfeld-Clauss S, Temm-Grove CJ, Bovenkerk JE, Pell CL, Johnstone BH, Considine RV, March KL. Secretion of angiogenic and antiapoptotic factors by human adipose stromal cells, Circulation. 109 (2004) 1292–1298. 10.1161/01.CIR.0000121425.42966.F1. [PubMed: 14993122]

[48]. Deponte M. Glutathione catalysis and the reaction mechanisms of glutathione-dependent enzymes, Biochim Biophys Acta. 1830 (2013) 3217–3266. 10.1016/j.bbagen.2012.09.018. [PubMed: 23036594]

[49]. Mangi AA, Noiseux N, Kong D, He H, Rezvani M, Ingwall JS, Dzau VJ. Mesenchymal stem cells modified with Akt prevent remodeling and restore performance of infarcted hearts, Nat Med 9 (2003) 1195–1201. 10.1038/nm912. [PubMed: 12910262]

[50]. Wang X, Zhao T, Huang W, Wang T, Qian J, Xu M, Kranias EG, Wang Y, Fan GC. Hsp20-engineered mesenchymal stem cells are resistant to oxidative stress via enhanced activation of Akt and increased secretion of growth factors, Stem Cells. 27 (2009) 3021–3031. 10.1002/stem.230. [PubMed: 19816949]

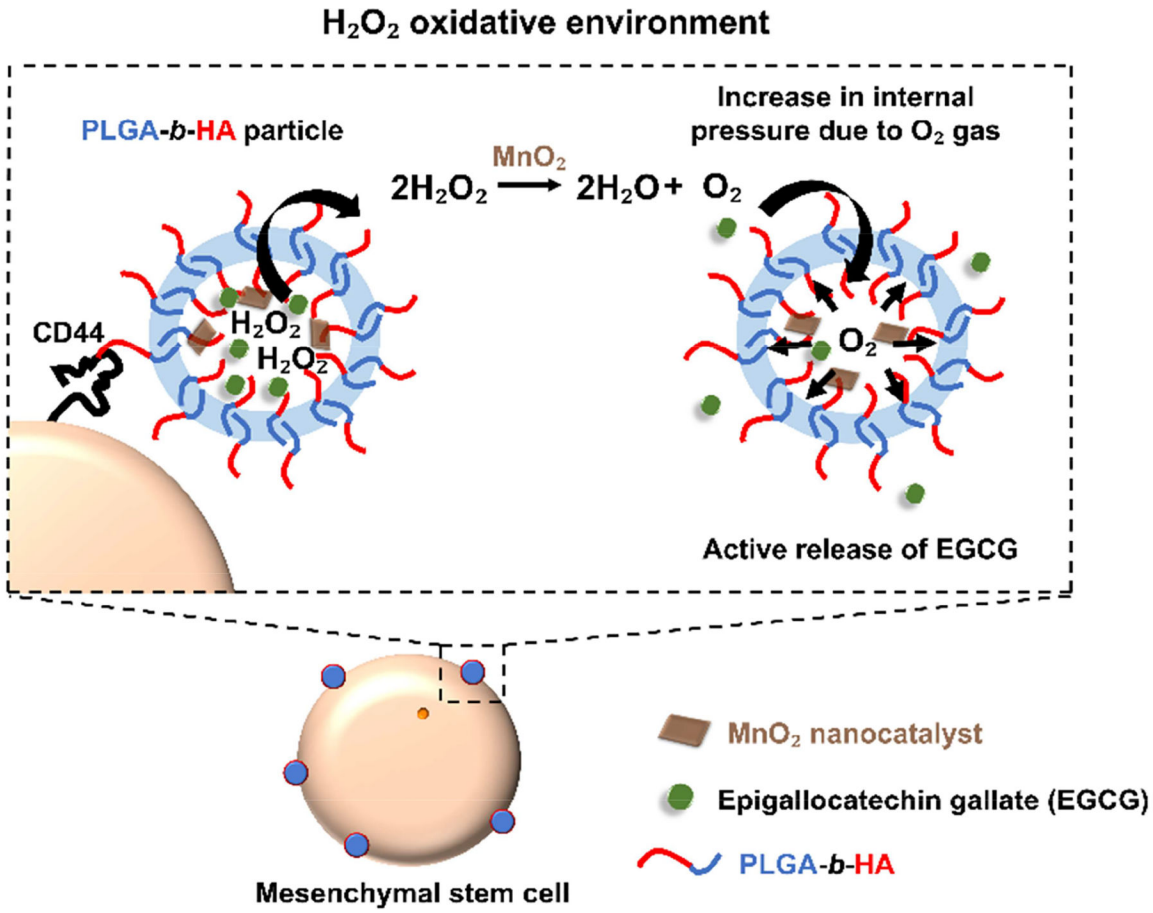

Figure 1.

In situ protection of mesenchymal stem cells in a H_2O_2-rich environment by tethering H_2O_2-responsive anti-oxidizing particles to cells. Stem cells are tethered with PLGA-*b*-HA particles containing antioxidant EGCG and MnO_2 nanocatalysts *via* HA-CD44 interactions. MnO_2 nanocatalysts catalyze the decomposition of H_2O_2 within the particles and the resulting O_2 gas increases the internal pressure. The O_2 gas pushes the EGCG molecules out of the particles, facilitating the rescue of stem cells from oxidative damage.

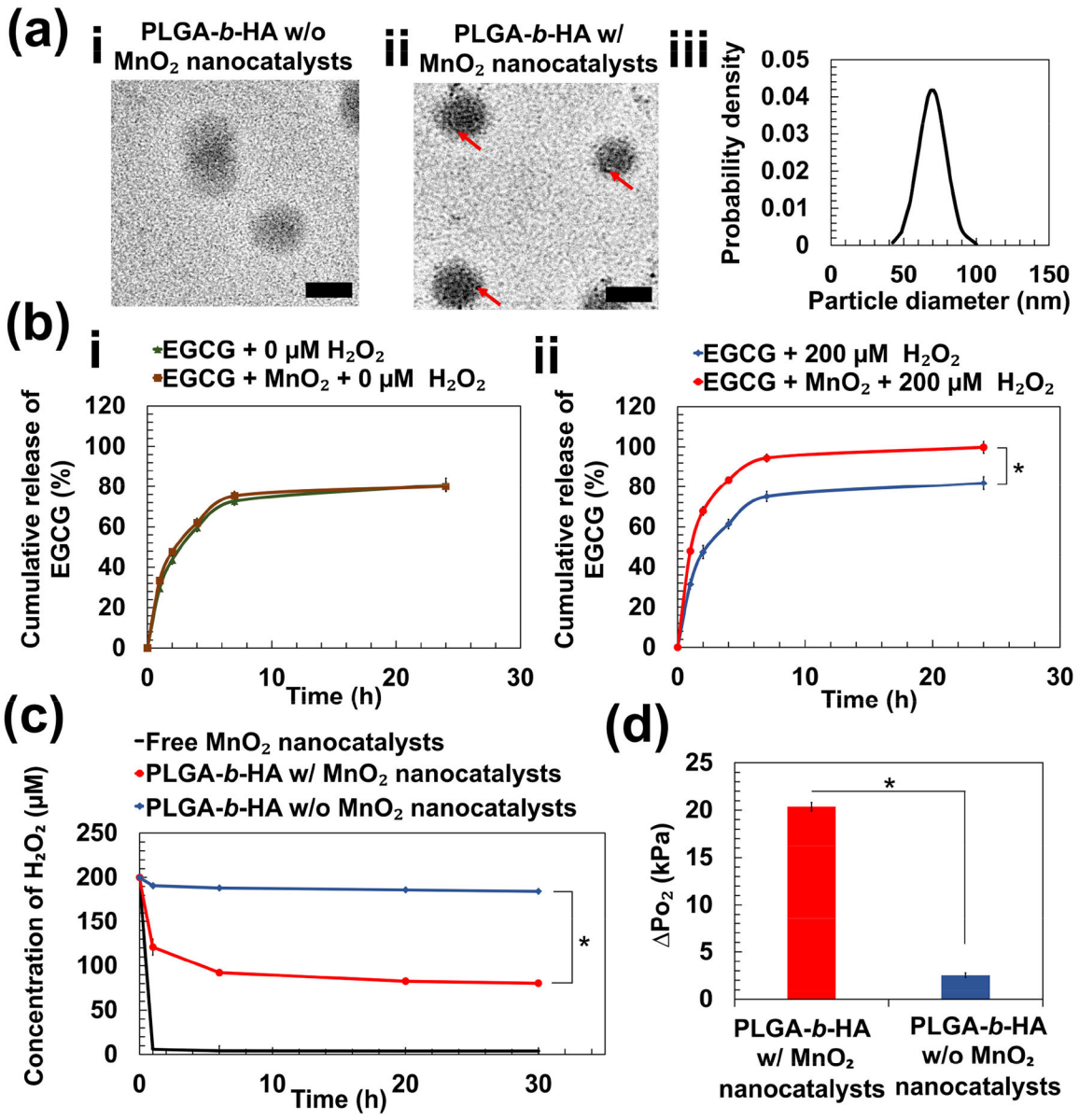

Figure 2:

Physical characterization of PLGA-*b*-HA particles containing EGCG and MnO_2 nanocatalysts. (a) Transmission electron microscopic images of particles loaded with EGCG (a-i) and particles loaded with EGCG and MnO_2 nanocatalysts (a-ii). Red arrows indicate the existence of MnO_2 nanocatalysts. Scale bar = 50 nm. (b) Release profiles of EGCG over 24 h at 37 °C. EGCG-loaded particles with and without MnO_2 nanocatalysts were immersed in either phosphate-buffered saline (PBS) (i) or PBS containing 200 μM H_2O_2 (ii). (c) The rate of change of H_2O_2 concentration in media containing free MnO_2 nanocatalysts and particles with and without MnO_2 nanocatalysts. (d) The increase in pressure of O_2 gas (ΔP_{O_2}) at 24 h due to generation of O_2 from the decomposition of H_2O_2. The values and error bars represent the average values and standard deviation of three individual samples per condition, respectively. * represents the statistical significance of the difference of value

for particles loaded with EGCG and MnO_2 nanocatalysts in PBS containing 200 μM H_2O_2 and that for each of the three other conditions. (* $p < 0.05$).

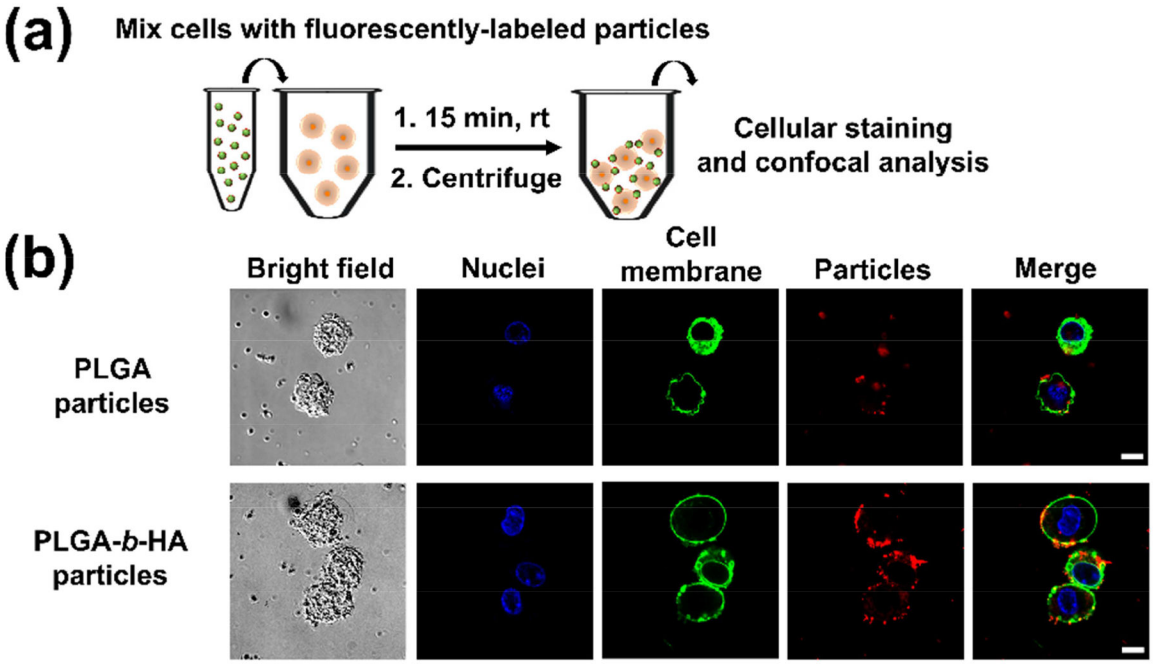

Figure 3:

Analysis of PLGA and PLGA-*b*-HA particles tethered to cells. (a) Schematic showing the procedure to tether particles onto stem cells for 15 min at room temperature, followed by centrifugation to remove unbound particles. The particles were labeled by loading bovine serum albumin conjugated with Rhodamine B (red). (b) Representative confocal images of the cells tethered with the particles. Cell nuclei and cell membrane were stained with Hoechst 33342 (blue) and DiO dye (green), respectively. Scale bar = 10 μm.

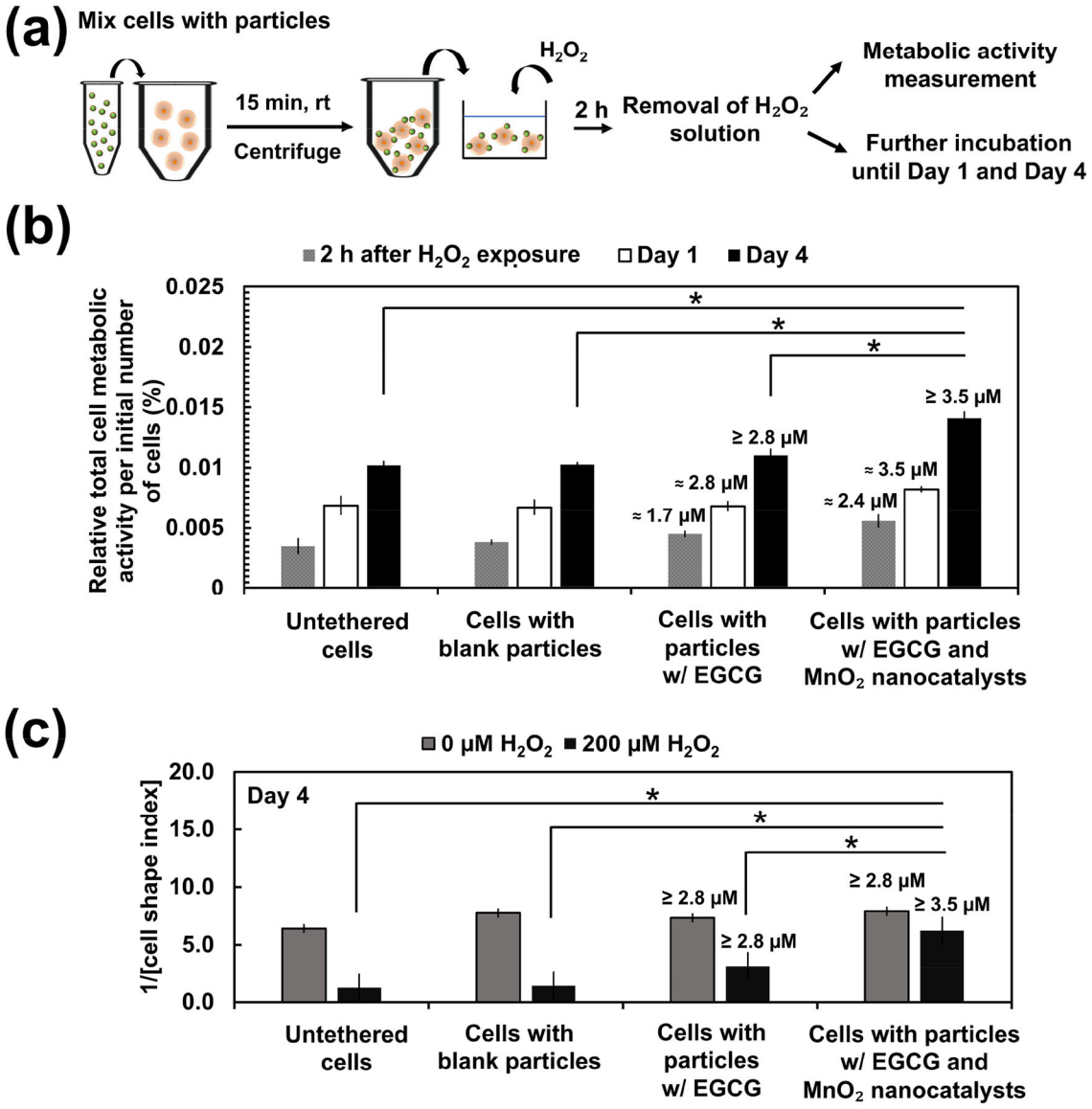

Figure 4:

Analysis of metabolic activity and morphology of stem cells in an oxidative environment. (a) Schematic demonstrating the procedure to assess the metabolic activity of stem cells seeded in the collagen gel. The cells were subsequently exposed to 200 μM H_2O_2 for 2 h. The H_2O_2 solution was then replaced with H_2O_2-free fresh culture media either for measurement of metabolic activity or for further incubation for 1 day or 4 days at 37 °C, 5% CO_2. (b) The overall metabolic activity per initial number of cells measured at different time points following exposure to 200 μM H_2O_2 for 2 h. The overall metabolic activity was expressed as the fraction of metabolically active cells with respect to the metabolic activity of groups treated in the same way but not exposed to H_2O_2. The values and error bars represent the average percentage of metabolic activity and standard deviation of three individual samples per condition, respectively. (c) The inverse of cell shape index of stem cells of various conditions on Day 4 after the H_2O_2 exposure for 2 h. The values and error bars represent the

average percentage of metabolic activity and standard error of 50 individual cells per condition, respectively. * represents the statistical significance in the difference of values between the indicated conditions (* $p < 0.05$). The numerical values noted above the bars are the estimated amount of EGCG released from the particles. The amount of EGCG released was estimated using the *in vitro* release profile of EGCG obtained in Figure 1b. The initial loading of EGCG was 3.5 μM.

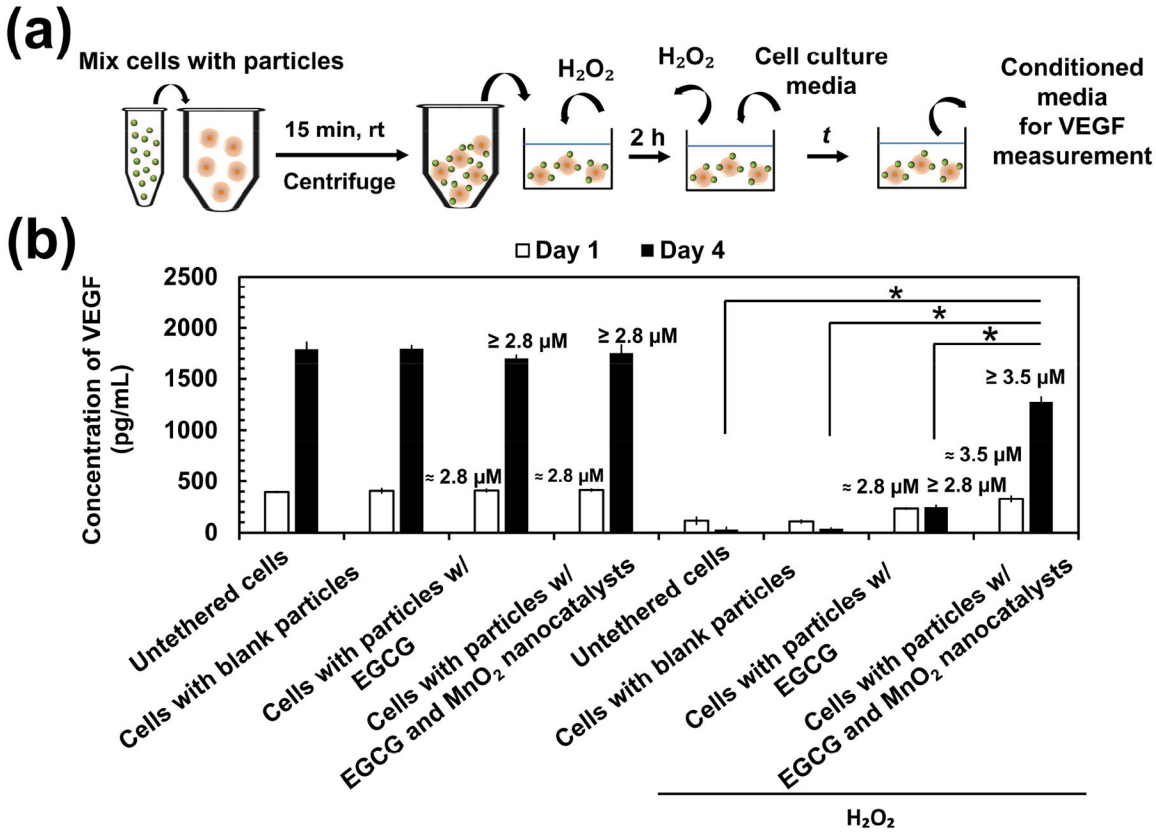

Figure 5:

Secretion activity of mesenchymal stem cells. (a) Schematic describing the procedure to evaluate cellular secretion activity. Stem cells were seeded in the collagen gel and incubated in media containing 200 μM H_2O_2 for 2 h. The media containing H_2O_2 was then replaced with fresh culture media and incubated for 1 day and 4 days before collecting the conditioned media to measure the VEGF concentration. (b) VEGF concentration in the conditioned media of the various conditions as noted in the plot. The values and error bars represent the average concentration and standard deviation of three individual samples per condition, respectively. * represents the statistical significance of difference in the values between the indicated conditions (* $p < 0.05$). The numerical values indicated above the bars are the estimated amount of EGCG released from the particles. The amount of EGCG released was estimated using the *in vitro* release profile of EGCG obtained in Figure 1b. The initial loading of EGCG was 3.5 μM.

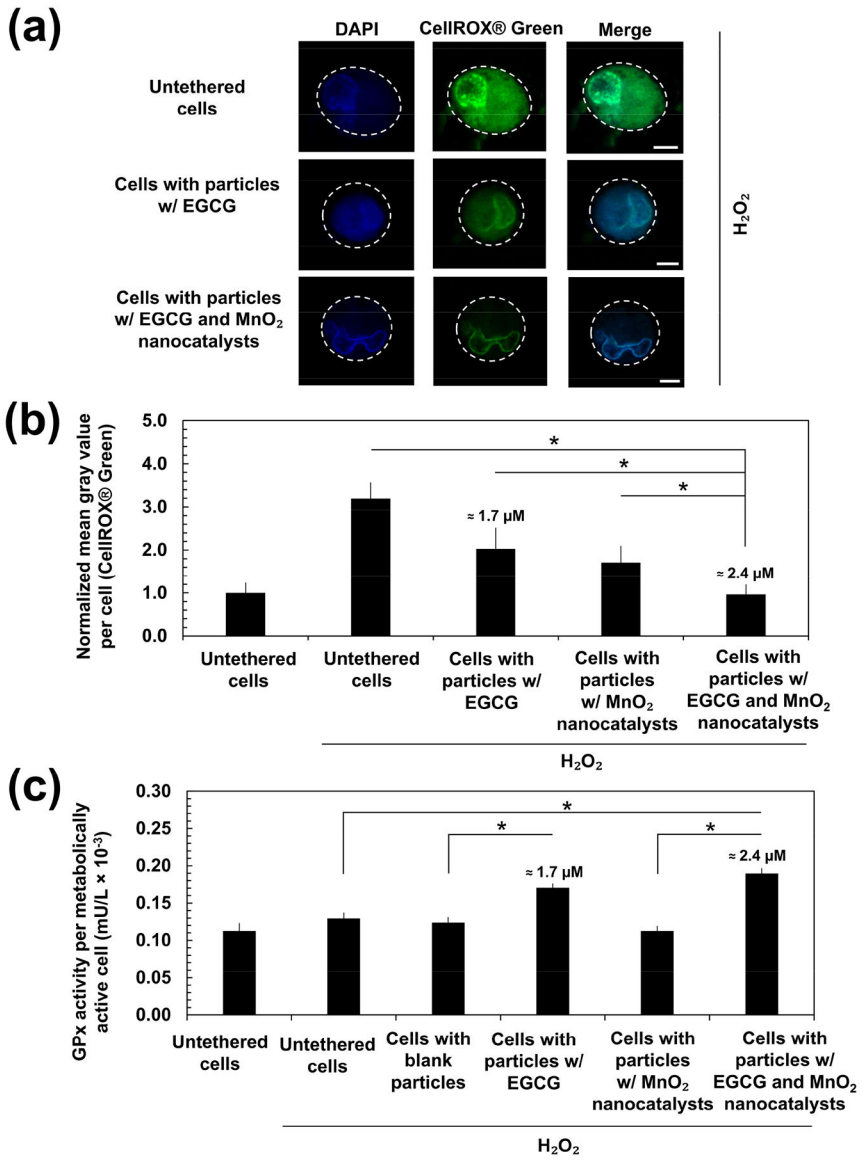

Figure 6:

Analysis of the intracellular oxidative stress level and the antioxidant enzyme glutathione peroxidase (GPx) activity. (a) Representative fluorescence images of the CellROX® Green in the stem cells for analysis of the intracellular oxidative stress. Cells were cultured in media containing 200 μM H_2O_2 for 2 h and imaged immediately. Scale bar = 5 μm. (b) Mean gray value of CellROX® Green per cell was quantified using the ImageJ Software. The green channel representing the CellROX® Green of the fluorescence images in (a) was first converted to 8-bit gray. The periphery of each cell was then manually traced to obtain the region of interest. The mean gray values within the region of interest was then obtained. The values were normalized with respect to that of stem cells which were not exposed to H_2O_2. These values and the error bars represent the average values and standard deviation from a minimum of five cells per condition, respectively. (c) Activity of GPx in stem cells following exposure to either culture media or media containing 200 μM H_2O_2 for 2 h. The

value of GPx activity was normalized with respect to the number of metabolically active cells in each condition. The values and error bars represent the average values and standard deviation of three independent samples, respectively. * represents the statistical significance in the difference of values between the two indicated conditions (* $p < 0.05$). The numerical values indicated above the bars are the estimated amount of EGCG released from the particles. The amount of EGCG released was estimated using the *in vitro* release profile of EGCG obtained in Figure 1b. The initial loading of EGCG was 3.5 μM.

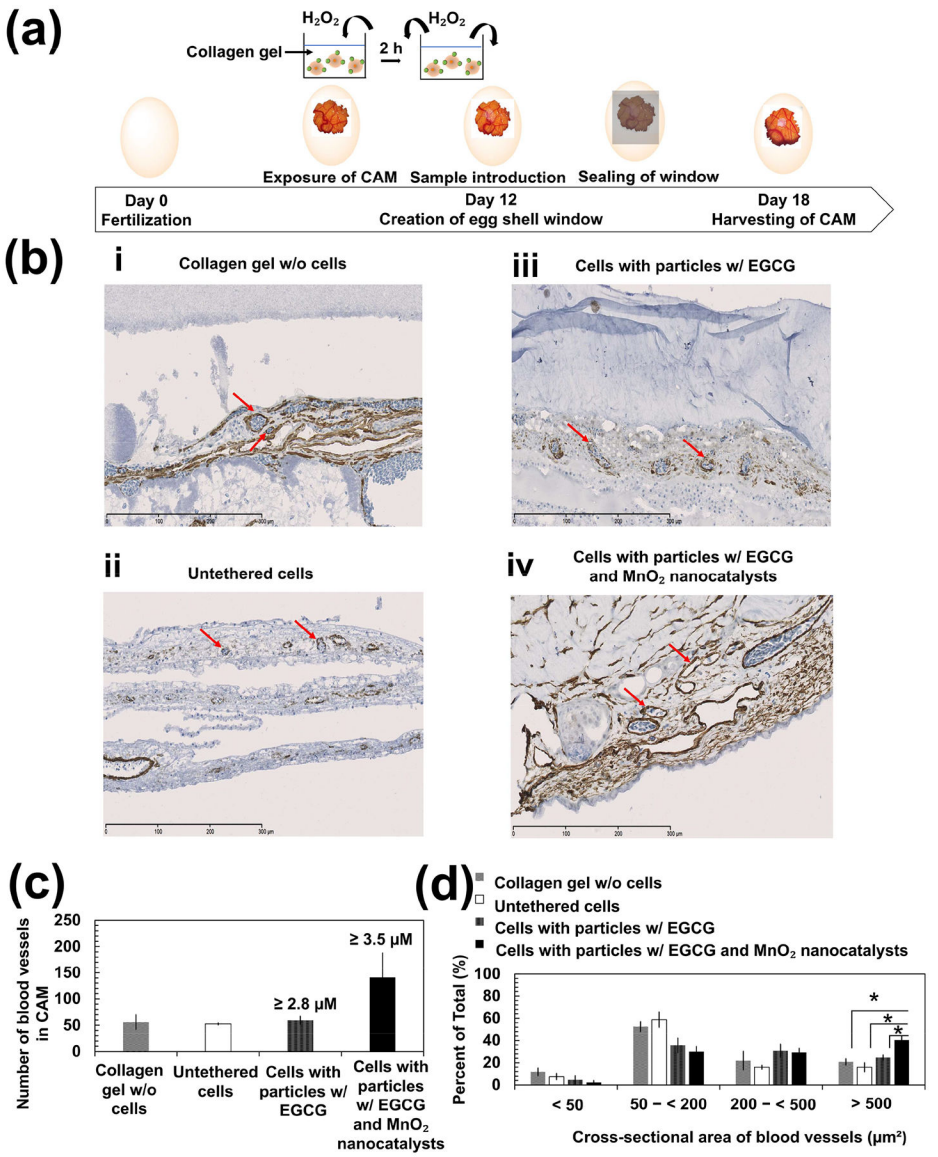

Figure 7:

In vivo chick chorioallantoic membrane (CAM) angiogenesis assay. (a) Schematic illustration of CAM assay. Eggshell was opened to expose CAM following 12 days of fertilization. Mesenchymal stem cells seeded within collagen gels were incubated in media containing 200 μM H_2O_2 for 2 h before implantation onto the CAM. The eggs were incubated for 6 days prior to harvesting the CAM. (b) Immunohistological analysis of the harvested CAM with an antibody to α-smooth muscle actin (red arrows). Images b-i, b-ii, b-iii, and b-iv represent cross-sections of CAM implanted with the collagen gel containing no stem cells, the collagen gel encapsulating untethered stem cells, the collagen gel encapsulating stem cells tethered with particles containing EGCG only, and the collagen gel encapsulating stem cells tethered with particles loading EGCG and MnO_2 nanocatalysts, respectively. Scale bar = 300 μm. (c) Quantification of the total number of blood vessels shown in the cross-sectional area of CAM where the sample was implanted on. The

numerical values indicated above the bars are the estimated amount of EGCG released from the particles. The amount of EGCG released was estimated using the *in vitro* release profile of EGCG obtained in Figure 1b. The initial loading of EGCG was 3.5 μM. (d) Quantification of the percentage of the number of blood vessels in the respective range of cross-sectional area with respect to the total number of blood vessels in the CAM. The values and error bars represent the average values and standard deviation from six to seven different regions of CAM per condition, respectively. * represents the statistical significance in the difference of values between the indicated conditions (* $p < 0.05$).